Investigation of integrated solid state nano-ionic metal–insulator–metal switches for electronically reconfigurable band-stop filter applications

Methapettyparambu Purushothama Jayakrishnan, Arnaud Vena, Brice Sorli, Etienne Perret

Investigation of Integrated Solid State Nano-Ionic Metal-Insulator-Metal Switches for Electronically Reconfigurable Band Stop Filter Applications

M. P. Jayakrishnan [1*], Arnaud Vena [2], Brice Sorli[2,] and Etienne Perret[1, 3]

[1] Univ. Grenoble Alpes, Grenoble INP[#], LCIS, 26000 Valence, France
[2] Institut d'Electronique et des Systèmes (IES), Université de Montpellier / CNRS, 34095 Montpellier, France
[3] Institut Universitaire de France, 75005 Paris, France
[#]Institute of Engineering, Univ. Grenoble Alpes
[*] jayakrishnan.mp@lcis.grenoble-inp.fr

Abstract: A proof of concept of application of Nano-Ionic Conductive–Bridging Metal-Insulator-Metal (MIM) switches in electronically reconfigurable band stop filters, through design, and experimental results are presented in this article. Two similar designs of band stop filters with different mechanism of operation are proposed herewith. One is a microstrip, resonant open stub based band stop filter and the other is a microstrip tuned shorted stub based band stop filter. Electrical length of the stubs in both these devices are tuned by an integrated MIM switch forcing them to resonate at different frequencies and thus achieving electronically switchable band stop filtering characteristics. Working mechanism of the devices is validated with the help of developed electrical equivalent circuit models. Analysis on time stability of switch states for 1000 minutes with affirmative results is also presented herewith. These devices are fabricated without any soldered electrical components and without the use of any clean room technologies, using proven low cost method, and are promising to work at very-low power and have the potential to be directly printed on low cost flexible substrates like paper, for potential disposable applications.

1. Introduction

Multi band reconfigurable filters would be of great use to present era of microwave and wireless communication [1]. Electronically reconfigurable multi band filters could benefit in increased versatility by reducing physical volume and signal processing budget of a system. A number of groups have successfully presented genius designs of electronically reconfigurable filters as in [1]–[4]. However, almost all these works utilize an active switching technology like a varactor or PIN diode or other solid state semiconductor switches to achieve the desired characteristics. These switches necessarily require a power source to maintain ON/OFF states and are generally active and volatile devices, and are integrated into the target device by techniques like soldering, which tend to degrade the RF performance of the circuit to some extent.

In this paper for the first time (to the best of our knowledge) we present the design and development of an electronically reconfigurable band stop filter using non-volatile passive solid-state nano-ionic metal-insulator-metal switches integrated to a planar filter topology, without any techniques like soldering. A MIM switch is a memristive switching technology initially identified as memory technology named Conductive Bridging Random Access Memory (CBRAM), derived from the concept of memristive switches called programmable metallization cells (PMC) [5]. As indicated by the name a MIM switch is a three layer switch (Metal − Insulator − Metal) similar in construction to a parallel plate capacitor, in which a layer of solid ion-conductor (which is an electronic insulator) is sandwiched by a layer of electrochemically asymmetric electrode pairs. One of the electrodes is an active ion-donor like silver or copper and the

other is a relatively inert ion-acceptor like aluminium or gold. The peculiarity of this presented switching technology is that it does not require a power source to maintain its state, once a set(ON)/reset(OFF) state is achieved using short low–power DC pulses, making it a fully non-volatile and solid-state switching technology. With highlights to non-volatility, it has been proved recently that MIM switches are promising candidates as next generation of passive RF-switches and renders smooth performance up-to 40GHz [6]. In black and white, non-volatility gives a special contrast to this switching technology in comparison to classic RF switches like MEMS or semiconductor solutions like PIN and Varactors. Possible list of ion-conductors for MIM applications include materials like chalcogenide glass [7], Hafnium dioxide [8], mouldable polymers like PMMA[9], Nafion [10] and even an air gap with precisely controlled electrode spacing [6]. A recent literature on MIM switches using in house fabrication techniques, reports more than 2000 cycles of operation [9], which is quite an acceptable number at the budding stage of a technology. CBRAM or MIM switch is identified to have more versatility of application, and lesser complexities in terms of ease of fabrication in comparison to other members of the PMC family like the Phase Change Memory (PCM) [11], [12] devices. Although most of the above cited RF-switching solutions including PCM and MIM require 'clean room' technologies for fabrication, [10], [13], [14] report a process for fabrication of Nafion based MIM RF switches using ambient laboratory

conditions, similar to an industrial environment, and notably without the need for any 'clean room' technologies, on classic as well as flexible substrates like paper. Such a construction is possible by the unique properties of polymer ion-conductors like Nafion[15], which could be easily transformed to layers of required thickness, without any high temperature processes. Another notable feature of this technology is that the switches could be potentially printed layer by layer along with the metallic structures, using polymer and metallic inks. This would be a giant step for the new trend of low power and passive disposable RF electronics[16] in near future.

Here we address the application of MIM switches in electronically reconfigurable band stop filter applications, in which the switch is implicitly integrated and fabricated along with the microstrip filter structure.

2. Analysis of Proposed Design

Proposed topology of filters is a stub loaded microstrip line as shown in Fig.1. Load stub is integrated with a MIM switch that tunes the electrical parameters and thus forces the stub to resonate at a particular frequency. The MIM switch is formed between the overlapping sections marked 'w3' and 'w4' in Fig.1, sandwiching a 600nm thick layer of Nafion. At resonance, most of the power input to Microstrip line is short circuited to ground through the stub, resulting in band stop characteristics. Design N1 is a microstrip line, loaded with a shorted stub and an integrated MIM switch. Design N2 is a microstrip

line loaded with an open circuited stub (with integrated MIM switch), which resonates similar to a quarter-wavelength resonator. Fig.2 shows the photographs of fabricated devices with microphotographs of switch areas in the inset. In N1 the stub is short circuited by connecting it to the ground plane of SMA connector as shown in Fig.2. The MIM switch is fabricated layer by layer using an optimized technique reported in [10]. Copper and aluminium forms active and passive electrodes and Nafion is the ion-conducting and electronic insulating layer, as shown in the inset of Fig.1.
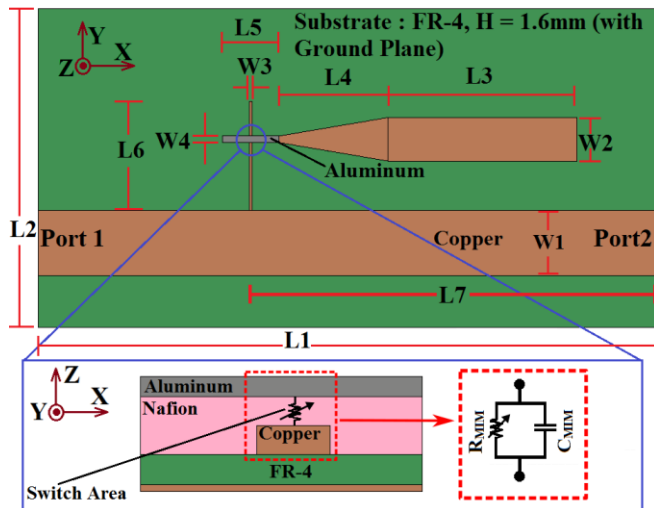

Fig. 1. Topology of Band Stop Filters. (W1=3mm, W2=2mm, W3=0.1mm, W4= 0.3mm, L2=18mm, L4=5mm, L5=2.6mm, L6=5mm. N1: Shorted Stub BSF, L1=28mm, L3=3.85mm, L7=14mm. N2: Open Stub BSF, L1=40mm, L3=14.7mm, L7=30mm).

The switch is operated using optimized DC voltage pulses [10] applied directly through the SMA connector for N1 and to the metallic parts using ordinary crocodile clips for N2. Proposed design is first simulated using CST microwave studio. A lumped resistor with values similar to experimented switch resistances is used to operate the MIM switch. Working mechanism of the band stop filters could be explained with reference to developed electrical equivalent circuit. This is a simple model which gives a good insight into the mechanism of operation of the presented device. A MIM switch could be represented using an RC parallel network (as shown in Fig.1) of which C_{MIM} is similar to capacitance calculated from geometry of the switch and R_{MIM} is similar to filament resistance measured across the switch electrodes [10], [13]. An open circuited resonant stub loaded on to a microstrip transmission line could be modeled as a serial RLC network as shown in Fig.3 [17].
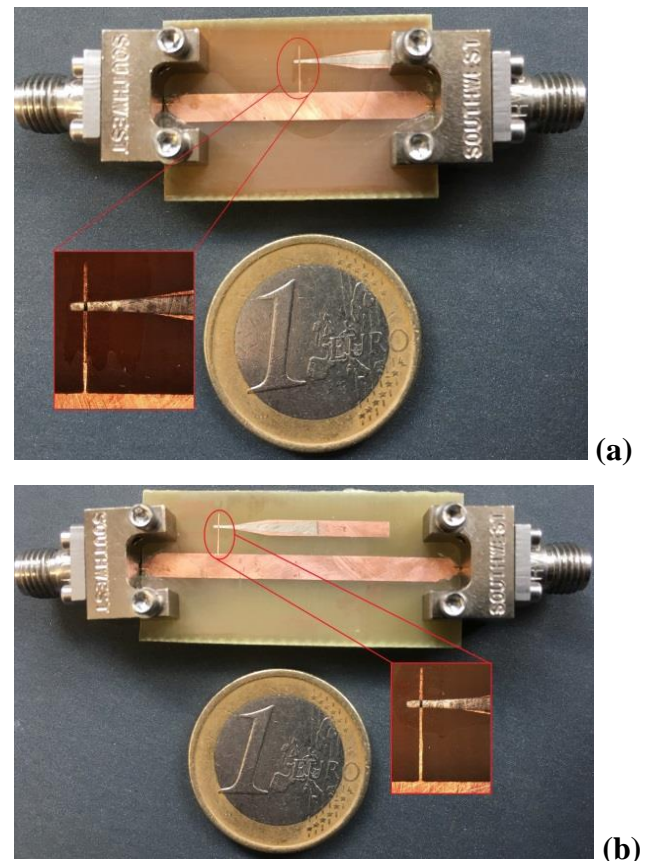

(a)

(b)

Fig. 2. Photographs of fabricated filters with microphotograph of MIM switch in the inset. (a) Shorted Stub BSF (N1). (b) Open Stub BSF (N2).

1. Design N1

In case of N1, the device could be approximated as a series RL network in series

with parallel RC approximation for the MIM switch as shown in Fig.3 (a). The stub is not resonant in ON state of the switch, in the targeted bandwidth (or in absence of switch – direct connection between two arms of the cross marked by 'w3' and 'w4' in Fig.1) and resonates with a surface current pattern much less than a quarter-wavelength distribution in OFF state. Mechanism of operation of N1 is as follows. When the switch is in ON state, R_{MIM} is a very small value equivalent to a short circuit and most of the current flow is through this path, which is strong enough to ignore the path through C_{MIM}, thus the stub constitutes a non-resonant path, establishing all pass filter characteristics, as no much power is short circuited to ground through this path. When switch is in OFF state, R_{MIM} is a large resistance, close to an open circuit. This forces the current to flow only through C_{MIM} (or very negligible current flows through R_{MIM}) and the stub, resulting in a resonant circuit formed collectively by C_{MIM}, R_{SS}, and L_{SS}. During this resonance, most of the power originating from port 1 (or port 2) of microstrip line is short circuited to ground exhibiting band stop characteristics around resonance frequency.

2. Design N2

For N2, equivalent circuit could be modeled as an RLC serial network [17] for open circuit stub, in series with parallel RC equivalent for the MIM switch as shown in Fig.3 (b). Surface currents show a distribution similar to quarter wavelength at resonance, for both states of the switch for this design in CST simulation. Fig.4 shows the surface current distribution on the stub

at a resonance frequency which constitutes stop band (2.010GHz, OFF state), and at a non-resonant frequency in pass band (1.42GHz, OFF state). Mechanism of operation of N2 is also similar to above theory for different switch state of MIM cell, except that in this case, the stub is long enough to exhibit a resonance, and is approximated by an RLC serial network. This design thus has a band stop behavior in both states of the switch, but at different frequencies, depending on the net value of capacitance due to C_{MIM} and C_{OS}. During ON state of MIM switch, resonance depends only on R_{OS}, L_{OS}, and C_{OS}. When MIM switch is OFF, C_{MIM} is connected in series to C_{OS} thereby reducing net capacitance and shifting resonance to a higher frequency.
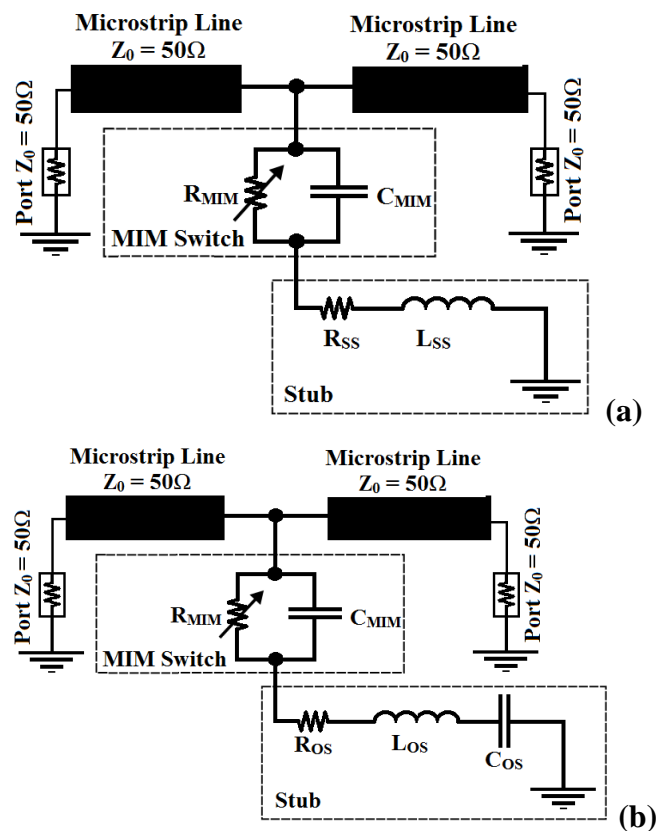

Fig. 3. Electrical Equivalent Circuits.
(a) N1. (b) N2.

3. Results

RF response of both devices is recorded using Agilent ENA E5061B Network Analyzer, using ordinary Short-Open-Load-Thru calibration. Fig.5 and 6 shows respectively the measured RF response of N1 and N2, along with results of full wave simulation and electrical equivalent circuit simulations. A triangular pulse of peak voltage +16V/0.5mA and a negative square pulse of -20V/150mA are used respectively to switch the devices ON and OFF similar to as reported in [10]. ON and OFF state resistance of MIM switch is in range of 1Ω-30Ω and 1MΩ-300MΩ respectively for most of the cycles. Table 1 shows optimized values of lumped components of electrical equivalent model of N1 and N2, through fitting with experimental results. This is done using CST Microwave Studio, in schematic mode. Values of R_{MIM} is similar to experimentally obtained filament resistance values of MIM cell, measured at DC using a source meter, and C_{MIM} is similar to calculated parallel plate capacitance due to geometry of electrodes and dielectric properties of ion-conductor [18] used.

TABLE I Electrical Model of Reconfigurable Band Stop Filters

Parameters (N1)	Shorted Stub BSF (N1)	Parameters (N2)	Open Stub BSF (N2)
R_{MIM}	21Ω /1MΩ*	R_{MIM}	1Ω/1MΩ*
C_{MIM}	1.4pF	C_{MIM}	1.48pF
R_{SS}	9Ω	R_{OS}	5Ω
L_{SS}	8nH	L_{OS}	8.35nH
(*Respectively for ON and OFF states)		C_{OS}	1.5pF

N1 shows an insertion loss less than -2dB in pass band and an isolation greater than -11dB, with -10dB bandwidth of 80MHz in stop band. Similarly N2 shows an insertion loss less than -2dB in pass band, and an isolation greater than -14dB, with -10dB band width greater than 140MHz for both stop bands. One should note that these results are inclusive of effects of associated transmission line, feed lines and SMA connectors. We could see that the results of experiment are in good agreement with results of full wave simulation and electrical equivalent circuit.
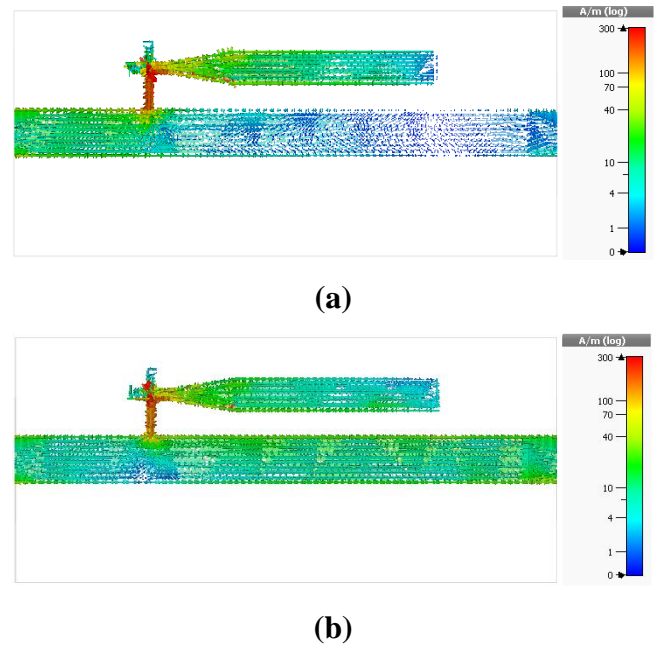

(a)

(b)

Fig. 4. Surface current distribution of Open Stub Band Stop Filter (N2): (a) Stop band (2.010GHz, OFF state), (b) Pass band (1.42GHz, OFF state).

Capacitance C_{MIM} is seen to have an acute control over the OFF state resonance frequencies of the filters. C_{MIM} could be varied by controlling the electrode area of MIM cell, determined by the width 'w3' and 'w4' (in Fig.1), for a given thickness of ion-conductor layer. For N2 this effect could be used to control the shift between ON and OFF state resonances as shown in Fig.7 (study using the electrical equivalent model).
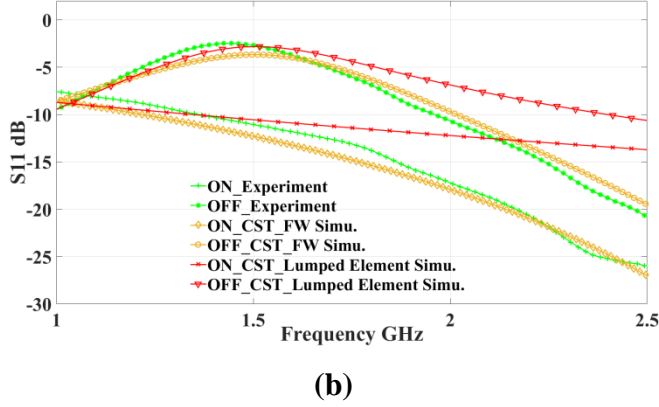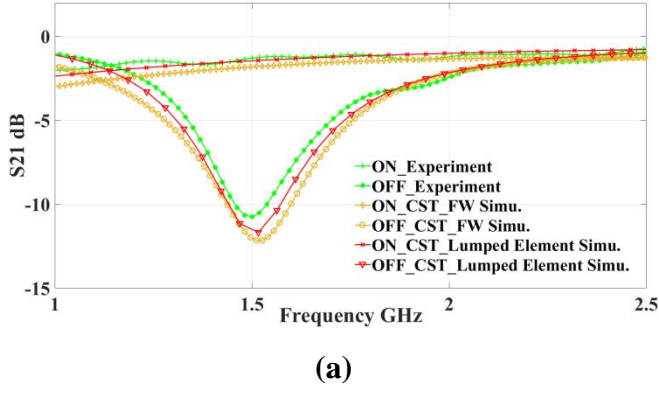
(a)

(b)

Fig. 5. RF-Response of Shorted Stub Band Stop Filter (N1): (a) S21, (b) S11.
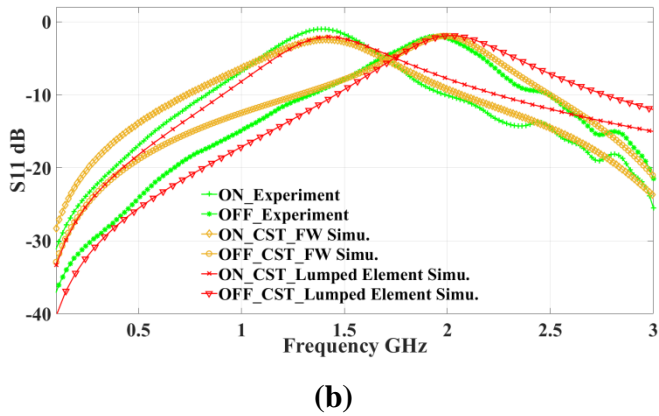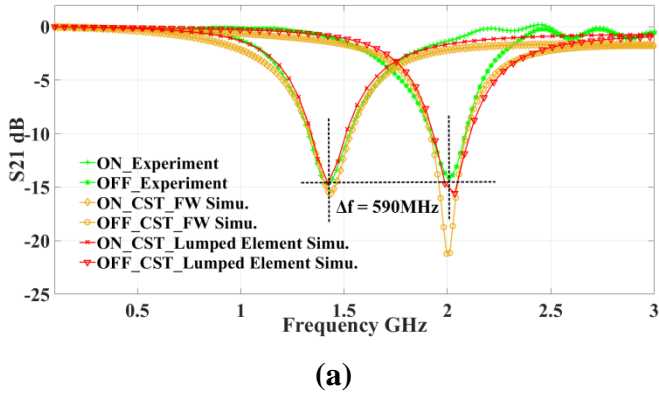

(a)

(b)

Fig. 6. RF-Response of Open Stub Band Stop Filter (N2): (a) S21, (b) S11.

In the presented case on this article, a 590MHz shift is achieved for C_{MIM} of 1.48pF (see Fig.6 a). Lower capacitance values and hence higher separation in resonance frequencies could be reached by finer widths of MIM electrodes, which are only limited by the least feature size of the available fabrication technique. Similarly for N1 this effect could be used to fine tune resonance for a given length of stub. One should also note that resonance frequency could be varied in gross by optimizing length of stub, 'L3' in Fig.1. However, the control on C_{MIM} could be used as an advantage in achieving a required filter characteristic of operation, utilizing the available physical space in a general design.

This design strategy could be represented mathematically as shown. Equation (1) shows the mathematical model for determining the resonance frequency 'F_r' of presented open stub band stop filter N2, which is similar to a quarter wavelength resonator. The effective length $L_{effON/OFF}$ of the stub could be represented as a function of a tune width (w_t) of electrode area of MIM switch, and a tune length of stub (L_t) for both ON (2) and OFF (3) state of MIM switch. The tune width and tune length chosen here are respectively 'w4' and 'L3' in Fig.1.

$$F_r = \frac{c}{4\,L_{effON/OFF}\sqrt{\varepsilon_{eff}}} \tag{1}$$
$$L_{effON} = -0.8w_t + L_t + 25 \tag{2}$$
$$L_{effOFF} = -26w_t^2 + 32.7w_t + 0.5L_t + 11 \tag{3}$$

Here c is speed of light in vacuum in m/s and ε_{eff} is effective dielectric permittivity of substrate and is calculated to be 3.16 in the presented case.

This equation is optimized through non-linear multiple variable regression analysis using the method of least squares. This model is optimized as a function of simulation data and is valid for 'w_t' in the range 0.1 to 0.7mm and 'L_t' in the range 10 to 18mm. The maximum calculated error is 30 MHz and 110 MHz, respectively for ON and OFF state. Table II shows a comparison of resonance frequency values obtained experimentally and using (1) for the presented device.
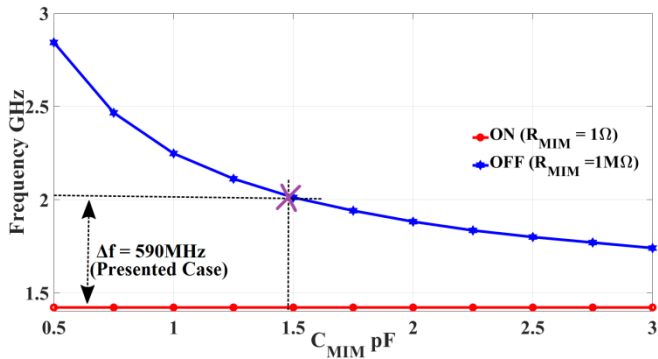

Fig.7. Dependence of Resonance Frequency on C_{MIM} (N2).

TABLE II Comparison of Experiment and Fit values of resonance frequency

	Experiment Fr(GHz)	Curve Fit (1) Fr(GHz)	|Error| (MHz)
ON	1.421	1.426	5
OFF	2.010	2.016	6

Next, time stability of the ON/OFF states of MIM switches were tested over time on a similar MIM switch and the result is depicted in Fig.8. It is observed that the ON/OFF states preserve their states for more than 1000 minutes. This result is an acceptable visualization about the time stability of the device. Further analysis on the maximum achievable time of switch state preservation is yet to be investigated and is in progress with the authors.
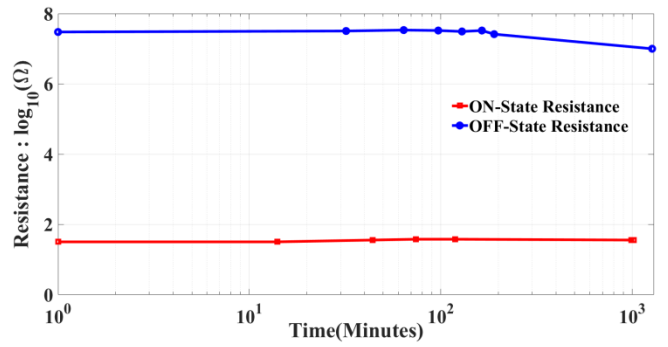

Fig.8. Time stability of MIM switch.

4. Discussions on Overcoming Limitations of Presented Design

The presented filter designs are of 1st order and are limited in bandwidth and stop band isolation. However, the presented data and results highlights feasibility and advantages of using proposed MIM switch technology for reconfigurable filter applications. This technique could also be extended without distinction to all types of planar filter topology which are optimized for specific filtering characteristics using well known classic design techniques [19], or using hybrid topologies [3], [20].

However, the operating bandwidth, roll-off rate (order) and stop band isolation in the presented case could be improved by introducing multiple identical resonator sections with integrated MIM switches for N1 and N2 (see Fig. 9). Simulation results of a filter similar in topology to N1, centred at 2.5GHz, shows an isolation of -10.5dB in stopband with a -10dB bandwidth of 80MHz and a -3dB roll-off rate of 5.8dB/GHz (see Fig. 10). On the addition of one and then two identical stubs with integrated switch, similar to first stub, shows respectively an enhancement as follows: isolation of -18.92dB and -23.41dB at centre frequency of stop band, -

10dB bandwidth of 380MHz and 580MHz, and -3dB roll-off rate of 7.6dB/GHz and 8.4dB/GHz, subsequently for two stubs and three stubs model. Topology of the simulated design and obtained S21 response are depicted respectively in Fig.9 and Fig.10. MIM switches were switched ON or OFF simultaneously for all stubs present, respectively, for a given ON or OFF state of the filter.

Presented filter topologies are also limited to single point tuning for N1, and dual point tuning for N2, in comparison to application using classic technology like PIN diodes [3], [20], which exhibit continuous tuning in a certain frequency range. However, the novelty of presented work is 'non-volatility' of proposed MIM switches, which cannot be implemented with PIN diode switches. Also in this case MIM switches are directly integrated into design without any techniques like soldering or conductive glue, which is not the case for classic application of PIN diodes.

On the other hand one could achieve multiple frequencies tuning in presented filters, similar to N2, by addition of multiple stub section, connected to the main resonant stub by integrated MIM switches (see Fig. 11). A simulation using design N2 was done by cascading in series two 5mm long stub segments at the open circuit end of stub, with electrical model of integrated MIM switch models, as shown in Fig. 11. Values of R_{MIM} and C_{MIM} of electrical model of MIM switch, are extracted from Table 1. This is done for simplicity and fast simulation, and could be replaced by real integrated MIM switches with optimized dimensions, at the time of application.

Simulation response of this design shows that stop band centre frequency could be tuned to 8 frequency points along a range of 900MHz from the first centre frequency, as shown in Fig. 12.
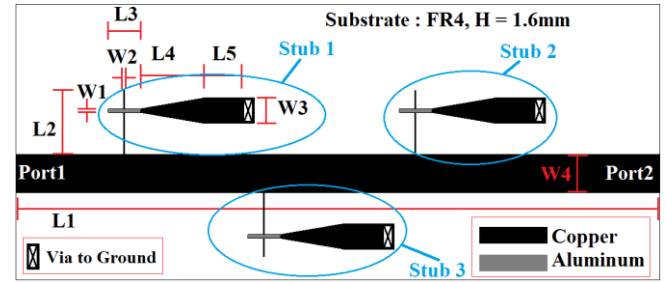

Fig.9. Reconfigurable shorted-stub band-stop filter topology with multiple (identical) resonator elements.
L1 = 60mm, L2 =5mm, L3 = 2.5mm, L4 = 5mm, L5 =3.85mm, W1=0.1mm, W2=0.1mm, W3=2mm, W4= 3mm.
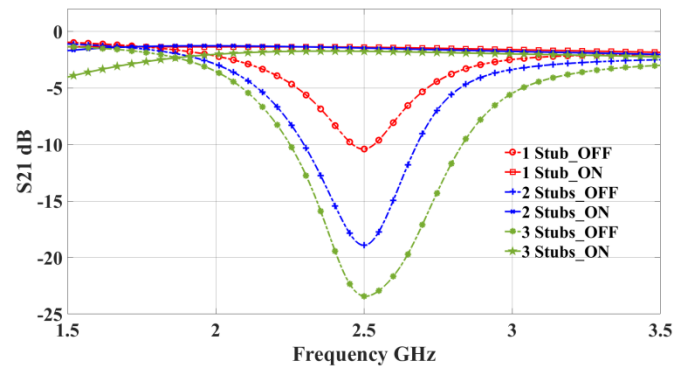

Fig. 10. Simulated S21 showing variation of bandwidth and roll-off rate with number of stub sections attached, for reconfigurable shorted-stub band-stop filter.

5. Conclusion

Potential ability of Nafion based Solid State Nano-Ionic Metal-Insulator-Metal switches for electronically reconfigurable filter applications are successfully demonstrated and presented in this paper. All the presented devices are tested for more than 50 cycles of operations and are still functional. We have previously demonstrated the fabrication of these kind of devices on paper

substrates using a similar technique [10]. This affirms that the presented design could also be fabricated without any soldered electrical components for low cost and flexible electronics, on substrates like paper.
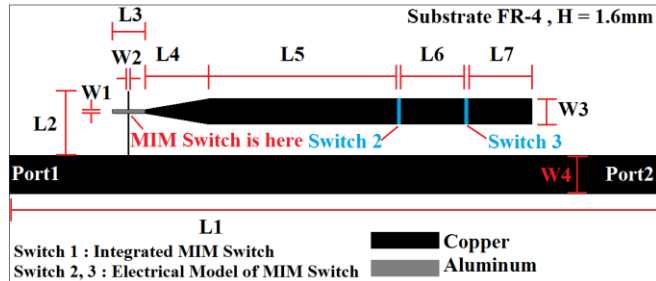

Fig. 11. Open-stub band-stop filter with multi frequency tuning.
L1 = 60mm, L2 =5mm, L3 = 2.5mm, L4 = 5mm, L5 =14.7mm, L6 = L7 = 5mm, W1=0.3mm, W2=0.1mm, W3=2mm, W4= 3mm.
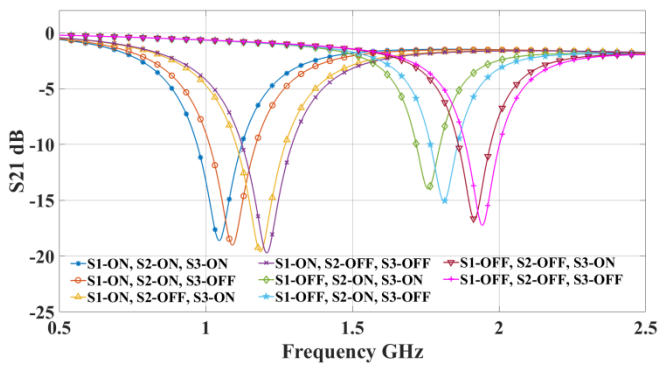

Fig. 12. Simulated S21 response of open-stub band-stop filter with multiple tuning sections for multi frequency tuning.
(In the legend of plot S1 – Integrated MIM switch, S2 – Switch 2, S3 – Switch 3)

The presented switching topology is a promising candidate for robust low-cost, low-power and low-weight applications, like in satellite systems for example. Authors are now focused on analysing underlying physics of the presented switching technology and in further understanding features, including effect of environmental factors like humidity, maximum

extent of achievable switching numbers and similar.

6. Acknowledgments

7. References

[1] J. Hong, "Reconfigurable planar filters," *IEEE Microw. Mag.*, vol. 10, no. 6, pp. 73–83, Oct. 2009.

[2] W. Feng, Y. Shang, W. Che, R. Gómez-García, and Q. Xue, "Multifunctional Reconfigurable Filter Using Transversal Signal-Interaction Concepts," *IEEE Microw. Wirel. Compon. Lett.*, vol. 27, no. 11, pp. 980–982, Nov. 2017.

[3] Z. Chen, S. Zhang, and Q. Chu, "Dual-band reconfigurable bandstop filter with independently controlled stopbands and constant absolute bandwidths," in *2017 IEEE MTT-S International Microwave Symposium (IMS)*, 2017, pp. 926–928.

[4] D. Psychogiou, R. Gómez-García, and D. Peroulis, "Fully-Reconfigurable Bandpass/Bandstop Filters and Their Coupling-Matrix Representation," *IEEE Microw. Wirel. Compon. Lett.*, vol. 26, no. 1, pp. 22–24, Jan. 2016.

[5] Michael N. Kozicki and William C. West, "Programmable metallization cell structure and method of making same," U.S. Patent 5,761,115, 02-Jun-1998.

[6] S. Pi, M. Ghadiri-Sadrabadi, J. C. Bardin, and Q. Xia, "Nanoscale memristive radiofrequency switches," *Nat. Commun.*, vol. 6, p. 7519, Jun. 2015.

[7] James Nessel and Richard Lee, "Chalcogenide nanoionic-based radio frequency switch," US 7.923,715 B2, 12-Apr-2011.

[8] M. Dragoman, M. Aldrigo, and G. Adam, "Phased antenna arrays based on non-volatile resistive switches," *Antennas Propag. IET Microw.*, vol. 11, no. 8, pp. 1169–1173, 2017.

[9] J. Jian, H. Chang, A. Vena, and B. Sorli, "Study and design of resistive switching behaviors in PMMA-based conducting-bridge random-access memory (CBRAM) devices," *Microsyst. Technol.*, vol. 23, no. 6, pp. 1719–1725, Jun. 2017.

[10] M. P. Jayakrishnan, A. Vena, A. Meghit, B. Sorli, and E. Perret, "Nafion-Based Fully Passive Solid-State Conductive Bridging RF Switch," *IEEE Microw. Wirel. Compon. Lett.*, vol. 27, no. 12, pp. 1104–1106, Dec. 2017.

[11] N. El-Hinnawy *et al.*, "Low-loss latching microwave switch using thermally pulsed non-volatile chalcogenide phase change materials," *Appl. Phys. Lett.*, vol. 105, no. 1, p. 013501, Jul. 2014.

[12] M. Wang, Y. Shim, and M. Rais-Zadeh, "A Low-Loss Directly Heated Two-Port RF Phase Change Switch," *IEEE Electron Device Lett.*, vol. 35, no. 4, pp. 491–493, Apr. 2014.

[13] M. P. Jayakrishnan, A. Vena, B. Sorli, and E. Perret, "Solid-State Conductive-Bridging Reconfigurable RF-Encoding Particle for Chipless RFID Applications," *IEEE Microw. Wirel. Compon. Lett.*, vol. 28, no. 6, pp. 506–508, Jun. 2018.

[14] J. Methapettyparambu Purushothama, A. Vena, B. Sorli, and E. Perret, "Electronically Re-Configurable, Non-Volatile, Nano-Ionics-Based RF-Switch on Paper Substrate for Chipless RFID Applications," *Technologies*, vol. 6, no. 3, p. 58, Jun. 2018.

[15] C. Heitner-Wirguin, "Recent advances in perfluorinated ionomer membranes: structure, properties and applications," *J. Membr. Sci.*, vol. 120, no. 1, pp. 1–33, Oct. 1996.

[16] B. S. Cook, T. Le, S. Palacios, A. Traille, and M. M. Tentzeris, "Only skin deep: Inkjet-printed zero-power sensors for large-scale RFID-integrated smart skins," *IEEE Microw. Mag.*, vol. 14, no. 3, pp. 103–114, May 2013.

[17] Muhammad Amin, Rashad Ramzan, and Omar Siddiqui, "Slow Wave Applications of Electromagnetically Induced Transparency in Microstrip Resonator," *Sci. Rep.*, vol. 8, pp. 1–13, Feb. 2018.

[18] Z. Lu, M. Lanagan, E. Manias, and D. D. Macdonald, "Two-Port Transmission Line Technique for Dielectric Property Characterization of Polymer Electrolyte Membranes," *J. Phys. Chem. B*, vol. 113, no. 41, pp. 13551–13559, Oct. 2009.

[19] David M. Pozar, *Microwave Engineering*, 3rd ed. United States of America: John Wiley & Sons,Inc, 2005.

[20] G. Chaudhary, Y. Jeong, and J. Lim, "Harmonic Suppressed Dual-Band Bandpass Filters With Tunable Passbands," *IEEE Trans. Microw. Theory Tech.*, vol. 60, no. 7, pp. 2115–2123, Jul. 2012.